Proceedings of the ASME 2021 International Technical Conference and Exhibition on Packaging and Integration of Electronic and Photonic Microsystems
InterPACK2021
October 26 – 28, 2021, Virtual, Online

InterPACK2021-73271

RACK-LEVEL THERMOSYPHON COOLING AND VAPOR-COMPRESSION DRIVEN HEAT RECOVERY: COMPRESSOR MODEL

Rehan Khalid
Dept. of Mechanical Engineering
Villanova University
800 Lancaster Avenue
Villanova, PA, USA, 19085
Email: r.khalid@villanova.edu

Raffaele Luca Amalfi
Thermal Management Group
Nokia Bell Laboratories
600-700 Mountain Avenue
Murray Hill, NJ, USA, 07974
Email: raffaele.amalfi@nokia-bell-labs.com

Aaron P. Wemhoff
Dept. of Mechanical Engineering
Villanova University
800 Lancaster Avenue
Villanova, PA, USA, 19085
Email: aaron.wemhoff@villanova.edu

ABSTRACT

This paper introduces a novel thermal management solution coupling in-rack cooling and heat recovery system. System-level modeling capabilities are the key to design and analyze thermal performance for different applications. In this study, a semi-empirical model for a hermetically sealed scroll compressor is developed and applied to different scroll geometries. The model parameters are tuned and validated such that the model is applicable to a variety of working fluids. The identified parameters are split into two groups: one group is dependent on the compressor geometry and independent of working fluid, whereas the other group is fluid dependent. By modifying the fluid-dependent parameters using the specific heat ratios of two refrigerants, the model shows promise in predicting the refrigerant mass flow rate, discharge temperature and compressor shaft power of a third refrigerant. Here, the approach has been applied using data for two refrigerants (R22 and R134a) to achieve predictions for a third refrigerant's (R407c) mass flow rate, discharge temperature, and compressor shaft power, with normalized root mean square errors of 0.01, 0.04 and 0.020, respectively. The normalization is performed based on the minimum and maximum values of the measured variable data. The technique thus presented in this study can be used to accurately predict the primary variables of interest for a scroll compressor running on a given refrigerant for which data may be limited, enabling component-level design or analysis for different operating conditions and system requirements.

Keywords: Data centers, Electronics cooling, Liquid-cooling, Mathematical modeling, Modeling, Thermal management of electronics

NOMENCLATURE

c_p	specific heat ratio at constant pressure, J/(kg K)
c_v	specific heat ratio at constant volume, J/(kg K)
h	specific enthalpy, J/kg
$\hat{h}$	heat transfer coefficient, W/(m^2 K)
k	ratio of specific heats, –
m	Number of output parameters, –
$\dot{m}$	mass flow rate, kg/s
n	number of data points, –
N	compressor shaft speed, rev/s
P	pressure, Pa
$\dot{Q}$	heat flow, W
R	ratio, –
$\hat{R}$	ideal gas constant, J/(kg K)
s	specific entropy, J/(kg K)
T	temperature, K
UA	overall thermal conductance, W/K
V	volume, m^3
V_s	swept volume, m^3
W	work, J
$\dot{W}$	mechanical power, W
$\dot{W}_{loss,0}$	electromechanical power loss, W
X	generic model output parameter

Greek Letters

α	model parameter, –
ϵ	heat exchange effectiveness, –
θ	error, –

Subscripts

ad	adapted
amb	ambient

comp	compressor
ex	exhaust
in	built-in
int	internal
loss	loss
meas	measured
mfr	manufacturer
p	pressure
r	refrigerant
sim	simulated
su	suction
v	volume/isochoric
w	wall

Acronyms

ACR	Air-Conditioning and Refrigeration
BPHE	Brazed Plate Heat Exchanger
DC	Data Center
EEV	Electronic Expansion Valve
HX	Heat Exchanger
ITE	Information Technology Equipment
LV	Liquid-Vapor
ORC	Organic Rankine Cycle
RMSE	Root Mean Square Error
NRMSE	Normalized Root Mean Square Error

1. INTRODUCTION

A commercially available scroll compressor features as part of a proposed novel cooling and heat recovery system for computer servers and telecom equipment. Figure 1 shows the proposed system, which comprises of two loops: i) Cooling loop, made up of the enclosed cabinet and its contents, the liquid-vapor separator (LV-separator) and a condenser (not shown in Figure 1) and ii) Heat Recovery Loop, which is a traditional heat pump and features the compressor under study.

The equipment to be cooled (computer servers in this case) are contained in an enclosed, air-cooled cabinet. The proposed thermal management solution is designed for legacy data centers (DCs) housing racks that contain servers mounted with air-cooled heat sinks. Server-level cooling is performed using traditional air-based cooling with active air-circulation via six fans located inside the cabinet. Thus, the design of the cooling system at the server-level is unchanged, which is preferred for many applications.

At the rack-level, traditional racks with perforated doors are replaced with an enclosed cabinet, thus differing from their legacy counterparts. The ITE is cooled by air that is continuously circulated within the cabinet, while the air itself is cooled via air-to-refrigerant heat exchange through a finned-tube heat exchanger that forms the evaporator of thermosyphon-based cooling system. A water-cooled brazed plate heat exchanger (BPHE) acts as the condenser for the cooling system. A reservoir tank (LV-separator) connects the two heat exchangers (HXs), thus physically separating the refrigerant liquid and vapor phases. The refrigerant can either reject heat directly through the condenser or be driven through a heat pump, thereby boosting its pressure (and temperature) before rejecting heat through the condenser for enhanced heat recovery.

If the water temperature exiting the condenser is near 75°C, then it can be used for significant economic activity generating tasks such as district heating networks, which are becoming increasingly popular across Europe [1], [2], [3], China [4] and Iran [5], [6]. Alternately, this high temperature water can be supplied as a service fluid to co-located process industries such as bottling and meat-packaging plants, used to heat indoor swimming pools [7] or used as potable water in the same or co-located buildings.

Lower temperature water exiting the condenser without use of a heat pump can be as high as 30 – 40°C, depending on the temperature of the saturated refrigerant inside the LV-separator. This can be used for low-temperature thermal tasks such as anaerobic digestion, warming greenhouses and water desalination [8], [9], [10].

The proposed system is advantageous when compared to traditional raised floor DC cooling, which presents disadvantages in terms of the electric energy consumed by the cooling system and the discharge of heat to the ambient without any intermediate use (typically high in quantity but low in quality). It also caters to the increasing average rack power density in DCs over the past three years [11], thus filling in a gap created by the growing need to switch to liquid cooling.

The proposed solution is a close-coupled technique where the air never leaves the rack (enclosed cabinet). It offers the following advantages when compared to air-cooling, RDHXs and modular cooling technologies:

i. Reduces the OPEX associated with CRAH units.

ii. Relies on self-regulating, passive thermosyphon-based cooling, thus eliminating moving parts such as pumps and gears, thereby reducing maintenance cost, increasing reliability of the cooling system, and reducing ITE downtime.

iii. Vapor from the LV-separator can be directly fed to a central rooftop condenser, which can be air-cooled to eliminate the expenditure of a chiller or cooling tower.

iv. Alternately, the vapor can be sent through a compressor (heat pump) before going through a water-cooled condenser or absorption chiller. The hot or cold water created can then be used for economic activity generation, as explained above.

v. Reduced carbon footprint via lesser CO_2 emissions (and possible financial gain if a local carbon tax is in place).

To that end, this study presents a mathematical model of a scroll compressor to better predict the performance of the proposed cooling and heat recovery system. The developed model can predict the compressor's performance for a variety of working fluids for which published data from the manufacturer or other external sources may not be available. Models for the finned-tube evaporator (cooling loop) and brazed-plate condenser (cooling and heat recovery loop) are published in two separate studies. The choice of working fluid is based on characteristics that influence the environment (ozone depletion potential – ODP and global warming potential – GWP) and system safety/performance (e.g. electrical conductivity and nominal boiling point) [12].

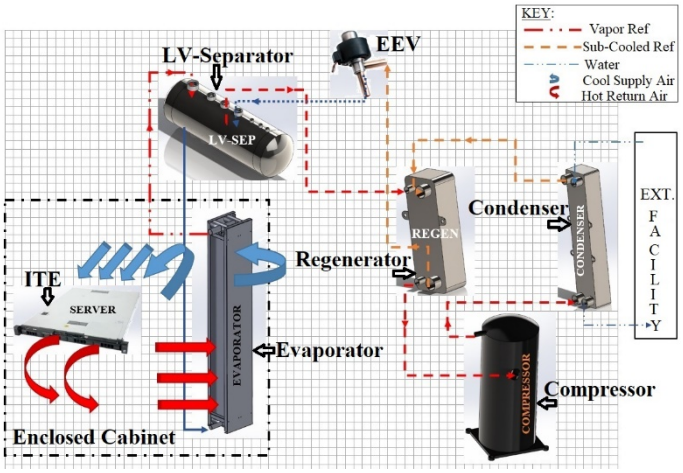

Figure 1: PROPOSED THERMAL MANAGEMENT AND HEAT RECOVERY SYSTEM

Scroll compressors are widely used in ACR applications, including heat pumps to boost the pressure and temperature of the working fluid, commonly a refrigerant, from the evaporator to the condenser pressure. Accurate models of these devices are important for system design and analysis, including predicting a compressor's discharge conditions based on its geometry, suction conditions and system working fluid.

This study uses the well-established model of Winandy et. al [13], developed for a given scroll compressor geometry with R22 as the working fluid, to predict the performance of a scroll compressor with a different geometry and working fluid.

Scroll compressors can be studied using techniques ranging from analytical to empirical. Byrne et al. [14] has provided a thorough literature review of the different models for scroll compressors published in the literature.

Analytical techniques for studying scroll compressors rely purely on the scroll geometry under consideration, such as the initial study conducted by Halm [15] and improved by Chen [16]. The analytical relations are complex and involve knowing the intricate details of the scroll geometry. These are rarely provided by manufacturers and are difficult to obtain otherwise due to inaccessibility of the internal scrolls (e.g., in a hermetically sealed compressor). Although Wang et al. [17] presented the relations for determining the geometry of a scroll compressor in detail, these are still difficult to use due to a lack of knowledge in scroll angles. Building on the work of Wang et al. [17], Oralli et al. [18] modified a scroll compressor to be used as an expander for an organic Rankine cycle (ORC).

Semi-empirical models have proved to be a popular method for studying scroll compressors due to their relative ease compared to analytical methods. These models do not require specific details of the internal scroll geometry, rather relying on measurements of the suction, exhaust, and internal stream conditions to gauge the internal working performance of the scroll geometry.

Winandy et al. [13] thereby retrofitted a scroll compressor with internal sensors to measure internal temperature and pressure as the working fluid moved along the scroll. Based on the gathered data, they were able to present a simplified semi-empirical model of a scroll compressor by modeling the compressor shell as a fictitious isothermal wall, against which internal and external heat transfer values could be calculated. The simplified model is meant to predict three important scroll compressor parameters, namely the discharge temperature, compressor shaft power draw and compressor allowable mass flowrate.

Cuevas et al. [19] pushed the applied pressure ratio for the same compressor to its limits, thereby confirming the efficacy of the simple model presented in [1]. Lemort [20] improved the model presented by Winandy et al. [13] by adding the pressure drop due to the presence of a reed type discharge valve commonly found in scroll compressors.

Lastly, purely empirical studies on scroll compressors have been performed. The major advantage is their relative accuracy for a given scroll geometry by eliminating the unknowns or assumptions prevalent in the other two techniques. The biggest disadvantage, however, is that these studies are limited to a specific scroll geometry and working fluid and cannot be generalized. Hence, they find limited use in applications involving analysis and performance prediction of scroll compressors installed in various systems. Prominent empirical studies performed for scroll compressors include those by Techarungpaisan et al. [21] , Kinab et al. [22] and by Byrne et. al [14] - [23].

Missing from these models is the capability to predict the performance of a scroll compressor whose geometry and/or working fluid differs from one for which test data is available. This study presents a simple yet accurate methodology to predict a scroll compressor's performance for exactly such cases, based on an existing semi-empirical scroll compressor model proposed by Winandy et al. [13]. This is useful under two scenarios: (i) when analytical models cannot be utilized due to a lack of detailed information about the scroll geometry; and (ii) when retrofitting existing systems or developing prototypes of new systems that rely on refrigerants for which manufacturer data for the intended refrigerant (using the same compressor) are not available. In such situations, the methodology presented in this study can enable one to predict the performance and discharge conditions of a given scroll compressor with a given working fluid. These predictions can further help in analyzing the overall performance of systems containing scroll compressors.

2. MODEL DEVELOPMENT

The physical and mathematical details of the semi-empirical scroll compressor model are provided in Winandy et al. [13] but are summarized here for completeness and to link them to the methodology developed in this study. A schematic of the scroll compressor model is shown in Figure 2. The working fluid, in this case a refrigerant, enters the compressor at the suction port, indicated by *su*, at conditions that can be easily measured experimentally or estimated analytically from conditions upstream (e.g., conditions at the L-V separator or regenerator

outlet, as per Figure 1). The state of the refrigerant at each point can be determined by either knowing or calculating the temperature and pressure of the refrigerant at each indicated point throughout the compressor. The mass flow rate of refrigerant entering the compressor is assumed to be unknown and is taken as an output of the compressor model.

It should be noted that the arrows in Figure 2 simply outline a generic path that the working fluid takes as it enters and flows through the compressor. The arrows are not meant to depict the actual flow path. Further, the identified points (**su**, **su$_1$**, **ad**, **ex$_1$** and **ex**) do not represent elevation with respect to a common datum and are spaced out for clarity.

The model divides the flow of the refrigerant through the compressor from suction, *su*, to discharge/exhaust, *ex*, into four sections, as indicated below:

1. Suction heat-up ($su \rightarrow su_1$)
2. Adiabatic and reversible (isentropic) compression ($su_1 \rightarrow ad$)
3. Adiabatic and constant volume compression ($ad \rightarrow ex_1$)
4. Discharge cool-down ($ex_1 \rightarrow ex$)

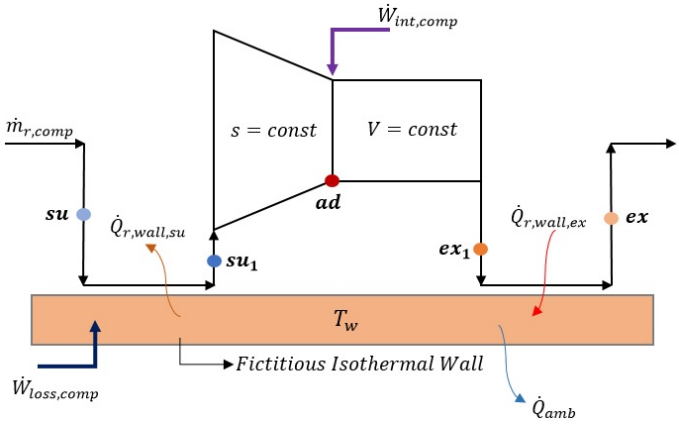

FIGURE 2: SCHEMATIC OF SCROLL COMPRESSOR MODEL - ADAPTED FROM [13].

Three heat transfer instances are involved in this process. During suction heat-up and discharge cool-down, heat exchange occurs between the refrigerant and the compressor shell, while ambient heat losses are characterized by heat exchange between the compressor shell and the compressor surroundings. To quantify these heat transfer mechanisms, the compressor shell is modeled as a fictitious isothermal wall at a constant, single temperature T_w. This simplified assumption leads to excellent agreement between the predicted and experimental results, as shown in Winandy et al. [13].

However, it is worth noting that for high evaporating and condensing temperatures not found in typical ACR applications, Cuevas et al. [19] demonstrated that the assumption leads to comparatively poor agreement between measured and predicted results. They therefore postulated that the wall temperature could be better represented by two constant temperatures instead of one. This approach would lead to separate temperatures for the suction and discharge sides of the fictitious compressor wall to allow for the larger temperature difference existing between the evaporating and condensing sides.

However, for purposes of this study, the single, constant wall temperature assumption leads to excellent agreement for the compressor geometry and refrigerants investigated, as demonstrated in Section 3 (in particular Scenario 3).

Compressor electromechanical losses associated with the motor winding are also accounted by the fictitious wall. These losses comprise of a fixed electromechanical power loss, denoted by $\dot{W}_{loss,0}$ and a loss term proportional to the internal work, $\alpha \dot{W}_{int}$, required for refrigerant compression, as presented first in the ASHRAE Toolkit Approach [24]. Both these parameters, namely $\dot{W}_{loss,0}$ and α, are identified parameters of the model, which need to be determined and optimized for a given geometry and choice of working fluid, details of which will be presented in the section on Model Tuning.

Application of the first law of thermodynamics on a control mass around the fictitious wall yields:

$$\dot{Q}_{ex} - \dot{Q}_{su} - \dot{Q}_{amb} + \dot{W}_{loss} = 0 \qquad (1)$$

where the change in internal energy of the control mass (i.e., the RHS of the equation) is zero at steady state and constant temperature, and the heat crossing the control surface going in and work done by the system are taken as positive. The parameters $\dot{Q}_{ex}, \dot{Q}_{su}, \dot{Q}_{amb}$ and $\dot{W}_{loss}$ represent heat transfer in the expansion process, suction, to ambient, and power loss, respectively.

The internal work term shown in Figure 2 is the power draw by the compressor that is required to compress the refrigerant from su_1 to ex_1. Part of the work is needed for isentropic compression of the refrigerant from state su_1 to ad, where the latter is the adapted pressure corresponding to the internal pressure ratio of the compressor because of the built-in volume ratio occurring as a result of the scroll geometry. The remaining portion of the internal power draw is used to compress the refrigerant from ad to ex_1, modeled as an adiabatic and isochoric process.

Application of the model for a given scroll geometry and choice of refrigerant is represented by the black box model of Figure 3. Input parameters include the suction temperature and pressure, which can be easily determined from experimental data without having to modify the compressor or from conditions directly upstream of the compressor. The discharge pressure can also be directly measured or taken as the condensing pressure. The nominal compressor shaft speed is required as an input to the model, which is readily available from the manufacturer. The intended working fluid is also an input to the actual model.

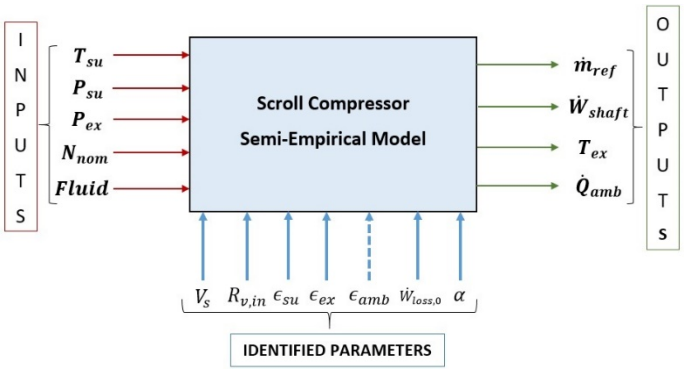

FIGURE 3: BLACK BOX MODEL OF SCROLL COMPRESSOR IDENTIFYING INPUTS AND OUTPUTS.

The outputs from the model are the mass flow rate of the refrigerant flowing through the compressor, the compressor shaft power and the refrigerant discharge temperature. Although the heat loss to the ambient is also shown as an output parameter of the compressor model in Figure 3, it is computed separately and is treated as a constant in the subsequent analysis, as explained in the section on Model Tuning. Secondary outputs (i.e., variables of interest) include the temperature rise of the refrigerant during the suction process, the temperature drop during discharge and the internal pressure ratio corresponding to the built-in volume ratio, $R_{v,int}$, which is an identified parameter of the model.

The process of going from the compressor inputs to outputs will be detailed in the Sections on Flow Sequence and Model Tuning. To summarize, however, the identified parameters of the model are first optimized separately before running the actual model, and the optimum values then fed into the compressor model to be used for further simulation.

2.1 Heat Transfer Analysis

2.1.1 Suction Heat Transfer. Analyzing the heat transfer on the suction side, the following expressions can be provided:

$$\dot{Q}_{su} = \dot{m}c_p\left(T_{su_1} - T_{su}\right) \tag{2}$$

$$\dot{Q}_{su} = \epsilon_{su}\dot{m}c_p(T_w - T_{su}) \tag{3}$$

where c_p is the specific heat capacity at constant pressure and $\dot{m}$ is the mass flow rate of the working fluid, where the subscript r has been dropped for ease. T represents the temperature at the location of interest while ϵ_{su} is the suction-side heat exchange effectiveness calculated as:

$$\epsilon_{su} = 1 - \exp\left(-\frac{(UA)_{su}}{\dot{m}c_p}\right) \tag{4}$$

where UA is the heat exchanger overall thermal conductance. Setting equations (2) and (3) equal yields:

$$T_{su_1} = \left[\exp\left(-\frac{(UA)_{su}}{\dot{m}c_p}\right)\right]T_{su} + \left[1 - \exp\left(-\frac{(UA)_{su}}{\dot{m}c_p}\right)\right]T_w \tag{5}$$

Or, in terms of ϵ_{su},

$$T_{su_1} = (1 - \epsilon_{su})T_{su} + \epsilon_{su}T_w \tag{6}$$

2.1.2 Exhaust Heat Transfer. Analyzing the heat transfer on the exhaust side, the following expressions can be reported:

$$\dot{Q}_{ex} = \dot{m}c_p\left(T_{ex_1} - T_{ex}\right) \tag{7}$$

$$\dot{Q}_{ex} = \epsilon_{ex}\dot{m}c_p(T_{ex} - T_w) \tag{8}$$

where ϵ_{ex} is the exhaust-side heat exchange effectiveness calculated as:

$$\epsilon_{ex} = 1 - \exp\left(-\frac{(UA)_{ex}}{\dot{m}c_p}\right) \tag{9}$$

Combining Eqs. (8) and (9) yields:

$$T_{ex_1} = \left[2 - \exp\left(-\frac{(UA)_{ex}}{\dot{m}c_p}\right)\right]T_{ex} - \left[1 - \exp\left(-\frac{(UA)_{ex}}{\dot{m}c_p}\right)\right]T_w \tag{10}$$

Or, in terms of ϵ_{ex}:

$$T_{ex_1} = (1 + \epsilon_{ex})T_{ex} - \epsilon_{ex}T_w \tag{11}$$

2.1.3 Ambient Heat Transfer. Finally, analyzing the ambient heat transfer, the following expression can be proposed:

$$\dot{Q}_{amb} = (UA)_{amb}(T_w - T_{amb}) \tag{12}$$

where UA is the overall thermal conductance and is calculated as follows:

$$(UA)_{amb} = \left(\hat{h}\right)\left(SA_{comp}\right) \tag{13}$$

Here, the heat transfer coefficient $\hat{h}$ is taken as a constant equal to 10 W/(m^{2}K), based on an average value of the HTC for free convection in gases [25]. Further, manufacturer specified dimensions can be used to calculate the surface area of the compressor exposed to the ambient. In the case of Copeland's scroll compressor with model number ZR61KCE-TF5-250, it comes out to be roughly 0.25 m^2.

2.2 Compressor Shaft Work Analysis

The compressor total power draw is computed as a sum of internal work and lost work:

$$\dot{W}_{shaft} = \dot{W}_{int} + \dot{W}_{loss} \tag{14}$$

The internal work, $\dot{W}_{int}$, is directly associated with the compression process and is computed assuming the compression is adiabatic and divided into two parts. The first part assumes adiabatic and reversible (isentropic process) compression with the refrigerant as an ideal gas with constant specific heats. The second phase assumes adiabatic compression at constant volume (isochoric process). The total internal work is thus computed as:

$$\frac{\dot{W}_{int}}{N} = W_{int} = W_{int,s} + W_{int,v} \tag{15}$$

$$W_{int} = W_s(su_1 \rightarrow ad) + \left(P_{ex_1} - P_{ad}\right)V_{ad} \tag{16}$$

$$W_{int} = \left(h_{r,ad} - h_{r,su_1}\right) + v_{r,ad}\left(P_{ex_1} - P_{r,ad}\right) \tag{17}$$

where N is the compressor shaft speed in Hz (revolutions per second). Each term in Eq. (17) can be determined as reported below. Starting from the conditions at su_1, the conditions (i.e., specific enthalpy h, specific entropy s, and pressure P) at point ad can be readily computed as follows:

$$h_{r,su_1} = h\left(T_{su_1}, P_{su_1}\right) \tag{18}$$

$$s_{r,su_1} = s\left(T_{su_1}, P_{su_1}\right) \tag{19}$$

$$s_{ad} = s_{r,su_1} \tag{20}$$

$$P_{r,ad} = R_{p,int}P_{r,su_1} \tag{21}$$

where the subscript 'r' is used to denote refrigerant and $R_{p,int}$ is the internal pressure ratio for the particular refrigerant corresponding to the compressor's built-in volume ratio (as a result of the scroll geometry), which itself is an identified parameter of the model and will be eventually optimized. The optimization of the six identified parameters is discussed in detail in the section titled Model Tuning, while a detailed methodology for computing the internal pressure ratio will be developed in the next section. From Eq. (17), $h_{r,ad}$ and $v_{r,ad}$ can be calculated as follows:

$$h_{r,ad} = h(P_{ad}, s_{ad}) \tag{22}$$

$$v_{r,ad} = v(P_{ad}, s_{ad}) \tag{23}$$

where v is the specific volume. Finally, the exhaust pressure at ex_1 can be determined as:

$$P_{r,ex_1} = P_{ex} + \Delta P_{ex} \tag{24}$$

where P_{ex} is an input to the model, corresponding to the condensing pressure, and ΔP_{ex},as well as ΔP_{su}, are determined from a linear fit to the exhaust and suction pressure drop data provided in Winandy et al. [13]. These data are gathered for a scroll compressor with a different geometry running with R-22 as the working fluid and will be detailed in the section on Model Tuning.

The compressor power losses are computed based on the ASHRAE Toolkit Approach [24] as the sum of a constant electromechanical loss term resulting from losses in the motor windings and a loss term proportional to the internal work. This is expressed mathematically as:

$$\dot{W}_{loss} = \dot{W}_{loss,0} + \alpha\dot{W}_{int} \tag{25}$$

$$\dot{W}_{loss,0}, \alpha, R_{v,int} > 0 \tag{26}$$

where both $\dot{W}_{loss,0}$ and α are identified parameters of the model and are eventually optimized. The total compressor shaft power is then simply as the sum of the internal work and the total losses, as expressed by Eq. (14).

2.2.1 Discharge Temperature. In order to determine the conditions at the compressor exhaust, point ex, the conditions immediately upstream (i.e., at point ex_1) need to be known. The pressure at ex_1 has already been computed using Eq. (24). The enthalpy at this point can be computed using the determined value of the internal work based on the energy balance as follows:

$$h_{r,ex_1} = h_{su_1} + \frac{\dot{W}_{int}}{\dot{m}} \tag{27}$$

Knowing the pressure and enthalpy then allows the temperature at point ex_1 to be determined. The exhaust or discharge temperature, T_{ex}, can then be computed using this upstream temperature value and the exhaust-side heat exchange effectiveness as:

$$T_{ex} = \frac{T_{ex_1} + \epsilon_{ex}T_w}{1 + \epsilon_{ex}} \tag{28}$$

The exhaust side heat exchange effectiveness can be suitably modified if the intended working fluid is different from the one used to tune the model. This topic will be explored in detail in the section on Model Validation.

2.2.2 Internal Pressure Ratio. The internal pressure ratio of the compressor for a given refrigerant and a given set of suction conditions is determined based on the isentropic compression of an ideal gas with constant specific heat. The conditions at suction and subsequent suction temperature rise and pressure change determine the conditions at point su_1. Thereon, the $'T\,ds'$ equations from thermodynamics can be applied to determine the relation between pressure and volume between point su_1 and point ad. Denoting the two state points with the numbers 1 and 2 respectively, and applying the Tds relations, results in:

$$s(T_2, v_2) - s(T_1, v_1) = c_v \ln\left(\frac{T_2}{T_1}\right) + \hat{R} \ln\left(\frac{v_2}{v_1}\right) \tag{29}$$

and

$$s(T_2, P_2) - s(T_1, P_1) = c_p \ln\left(\frac{T_2}{T_1}\right) - \hat{R} \ln\left(\frac{P_2}{P_1}\right) \tag{30}$$

For isentropic compression between states su_1 and ad, $\Delta s = 0$, which yields:

$$c_v\, ln\left(\frac{T_2}{T_1}\right) = -\hat{R} \ln\left(\frac{v_2}{v_1}\right) \tag{31}$$

and

$$c_p \ln\left(\frac{T_2}{T_1}\right) = \hat{R} \ln\left(\frac{P_2}{P_1}\right) \tag{32}$$

Dividing Eq. (32) by Eq. (31) yields

$$\frac{c_p}{c_v} \equiv k = -\frac{\ln\left(\frac{P_2}{P_1}\right)}{\ln\left(\frac{v_2}{v_1}\right)} \tag{33}$$

Since $\frac{P_2}{P_1} = \frac{P_{ad}}{P_{su,1}} = R_{p,int}$ (internal pressure ratio) and $\frac{v_1}{v_2} = R_{v,in}$ is the built-in volume ratio, simplification results in the following relation for the internal pressure ratio and built-in volume ratio:

$$R_{P,int} = R_v^k \tag{34}$$

where the specific heat ratio, k, is based on the conditions su_1, and R_v is short for $R_{v,in}$.

2.2.3 Suction and Exhaust Pressure Change. The compressor intended for this study is not equipped with internal sensors, nor is suction and discharge plenum data provided by the manufacturer for the intended compressor. Hence, in order to determine the change in pressure during suction and discharge, there was no other option but to resort to the data provided in Winandy et al. [13]. These data were collected for a compressor whose geometry and working fluid were both different from the ones intended for this study: the compressor in this study has a smaller swept volume with R-245fa as the working fluid compared to Winandy et al. [13]'s study with a larger swept volume and R-22 working fluid. Hence, a linear fit to the suction and exhaust pressure data presented in Winandy et al. [13] was utilized to determine the pressure changes for a given mass flow rate of the refrigerant. The results are presented graphically in Figure 4.

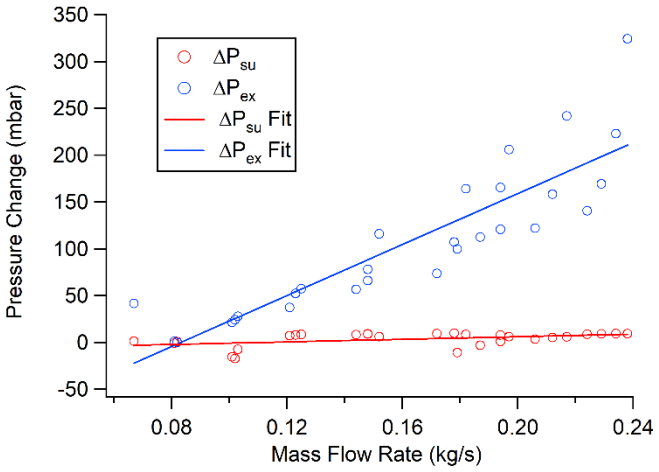

FIGURE 4: SUCTION AND EXHAUST PRESSURE CHANGE FOR R-22 AND A DIFFERENT COMPRESSOR.

Based on the linear fit to the suction and exhaust data presented in Figure 4, the pressure change during each process is given by:

$$\Delta P_{su} = 69.104\dot{m} - 7.6047 \tag{35}$$

$$\Delta P_{ex} = 1361.8\dot{m} - 113.27 \tag{36}$$

A linear fit yields R^2 values of 0.21 and 0.77 for suction and exhaust, respectively. The poor correlation for the suction data is compensated by the fact that the given suction pressure change is negligibly small with a maximum suction pressure rise of 15.4 mbar and a maximum suction pressure drop of under 10 mbar. Compared to the value of the suction pressure at point su, this pressure change value can practically be neglected without causing any significant change in the values calculated at point su_1. Similarly, the refrigerant always experiences a drop during the exhaust process based on the given data. Although the pressure change values are higher than the suction side, they are also negligible compared to the higher pressures existing on the discharge side (point ex). Hence, it is not essential to determine the absolute and correct value of these pressure changes, so the estimated values presented here are deemed sufficient.

3. Flow Sequence

Having established the necessary mathematical model for the scroll compressor, the flow sequence for making predictions using this model is shown as a flowchart in Figure 5.

The individual aspects include tuning the identified parameters using a fraction of the available test data, then feeding the values of the optimized parameters to validate the model using the remaining portion of the data not used for tuning. Note that this approach resembles that of training and validating machine learning-based algorithms, where tuning the identified parameters of the compressor model is equivalent to tuning the weights and biases of machine learning-based algorithms. If the testing error is within the specified tolerance, then the model is deemed to be acceptable for the intended geometry but with the refrigerant used for training and testing purposes.

At this stage, the model is ready to be used for the geometry of the intended compressor but with the refrigerant used by the manufacturer providing the tuning and testing data (referred to as base refrigerant from hereon). To make predictions for other refrigerants, the thermal properties of the intended refrigerant relative to the base refrigerant need to be taken into account. It will be shown in the section on Model Validation that this can be best done by taking the ratio of specific heat ratio (c_p/c_v) of the two refrigerants. Details for the individual aspects are presented in the following sections.

4. Model Tuning

Seven parameters are deemed as 'identified parameters' of the semi-empirical compressor model presented in Winandy et al. [13]. These identified parameters are internal to the model. To start computation, an educated guess for the initial value of these parameters is taken based on either the values presented in Cuevas et al. [19] or based on data provided by the manufacturer

for the intended compressor. The latter is the case when providing an initial guess for the swept volume, V_s, which provides a reasonably accurate starting guess.

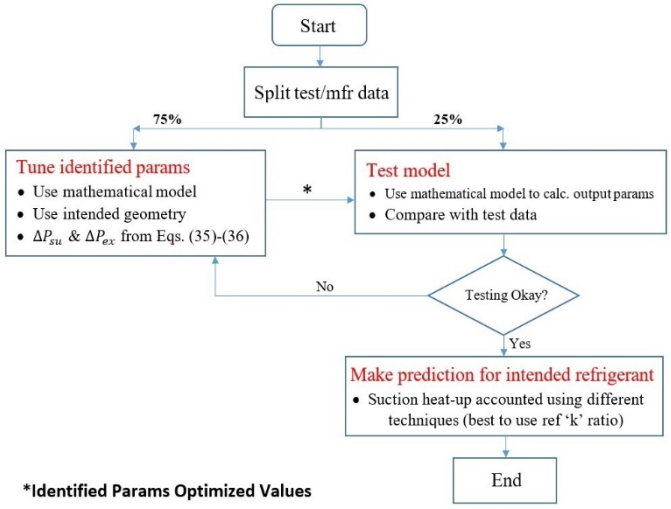

Figure 5: FLOW SEQUENCE FOR MAKING PREDICTIONS USING COMPRESSOR MODEL.

The model is tuned by minimizing the error of a pre-determined error function, which compares the simulated value of three output parameters against manufacturer provided test data, namely the compressor shaft power, discharge temperature and mass flow rate of the refrigerant. These output variables are calculated by the mathematical model described in Section 2. The final values of the identified parameters corresponds to the minimal value of the error function. The error is calculated as:

$$\theta = \sqrt{\frac{1}{n}\sum_{i}^{n}\sum_{j}^{m}\left(\frac{X_{ji,sim} - X_{ji,meas}}{X_{ji,meas}}\right)^2} \qquad (37)$$

where m corresponds to the number of identified parameters (6 in this case), and n corresponds to the number of data points chosen for model tuning.

Six parameters were identified as opposed to the seven indicated in Fig. 2 since ε_{amb} was calculated using an estimated value of $\hat{h}_{amb} = 10$ W/(m^2 K) based on the heat transfer accounting for natural convection and radiation, albeit small. The heat transfer coefficient and ambient temperature remained constant throughout the optimization process and the same values were used when running the model for testing and validation or prediction purposes. This was needed since test data were not available for the compressor wall temperature against which the simulated values could be compared.

The model is tuned based on data provided from the manufacturer, which includes 35 data points. Each data point provides values for compressor shaft power, refrigerant mass flow rate flowing through the compressor and refrigerant discharge temperature for a given condensing and evaporating temperature.

The first n = 27 data points were used to tune the model, while the remaining eight data points were used to test the model for R-134a, using the optimized values of the identified parameters obtained from the tuning phase. In this way, the semi-empirical compressor model provided in Winandy et al. [13] was tuned for a different compressor geometry and different choice of working fluid (R-134a instead of R-22 used in Winandy et al. [13]). Thus, R-134a is the base fluid in this case since manufacturer data used to tune and test the model were collected for this refrigerant.

The manufacturer data provide values for the input and output variables shown in Figure 3. However, values for some variables internal to the model were neither provided nor can they be deduced from the data. These include key aspects of the model such as the suction and exhaust pressure change and the suction temperature rise. The authors in Winandy et al. [13] were able to measure these by virtue of the sensors installed within the retrofitted model of the compressor that they used. Thus, for purposes of this study, the suction and exhaust pressure drop values were predicted from a linear fit to their data, as explained in Section 2.

For the suction temperature rise, the same strategy was initially intended. However, since the suction temperature rise is involved in predicting the mass flow rate of refrigerant flowing through the compressor using available values from the manufacturer, an iterative procedure was adopted where ΔT_{su} was initially assumed to be zero (i.e., $T_{su_1} = T_{su}$) and the predicted value of the mass flow rate compared against the manufacturer specified value. ΔT_{su} was subsequently incremented by a small amount, δT_{su}, and the procedure was repeated until the difference between the predicted and specified mass flow rate values were less than a pre-specified tolerance of 10^{-3}.

The final values for ΔT_{su} for different refrigerant mass flow rates were taken as those corresponding to the optimum values of the six identified parameters. The optimum values are listed in Table 1.

Figure 6 below graphically represents values for the suction temperature rise against the applied pressure ratio (P_{cond}/P_{evap}). The figure also shows a linear fit to this data, which is then used to predict the suction temperature rise for this compressor model with R-134a. These values are then used in the actual compressor model, where a modification factor is utilized to account for different choices of working fluid (refrigerant). In the case of the working fluid being R-134a, the factor would simply take the value of unity and the exact values predicted from the best-fit line of Figure 6 would be used. An appropriate choice for the modification factor will be explored in detail in the next section on Model Validation.

Finally, a sensitivity analysis, similar to that done by Cuevas et al. [19], was carried out on the model's identified parameters (listed in Table 1) for the same working fluid as used in [19] i.e. R-134a. The analysis is carried out by individually perturbing the optimized values of the identified parameters in the range

of ±5%, in increments of 1%. One parameter is perturbed at a time, while keeping the rest at their optimum value. The model response is gauged by the ratio θ/θ_0, where θ is the resultant error based on equation (37), using the perturbed value of the identified parameter, while θ_0 is the minimum error, found using the optimum values of all the parameters and already obtained at the conclusion of the model tuning process.

Results for the sensitivity analysis are presented in Figure 7, which shows that the model is most sensitive to the swept volume (or volume increment factor, K), followed by the built-in volume ratio, $R_{v,in}$, and then the proportionality factor for internal work loss, α. Figure 7 further shows that the model is practically insensitive to the suction and exhaust heat transfer efficiencies, while it is very slightly sensitive to the constant part of lost work, $\dot{W}_{loss,0}$.

These trends can be justified by the geometry of a scroll compressor, where the swept volume of the gas is key in determining the pressure rise that is going to be achieved. Since the manufacturer specified swept volume is not known with certainty, even a small value of the increment factor, K, causes a major change in the total swept volume and thereby the details of the compression process. Similarly, the internal volume ratio, $R_{v,in}$, is important and has the second largest influence. This volume ratio gives rise to an internal pressure ratio, as expressed by Eq. (34), which subsequently dictates the compression process. Optimum compression is achieved when the applied external pressure ratio is equal to the internal pressure ratio to prevent under or over-compression [13].

This trend agrees closely with that presented in [19], except for the trend for the constant loss term, which is seen to be practically insensitive to a change in the optimized parameter, following the same trend as the two heat transfer efficiencies [19]. Based on the sensitivity trends agreement between [19] and the current study, it is reasonable to assume that the same general trend would be followed for the scroll compressor used for this study, regardless of the choice of working fluid.

TABLE 1: OPTIMUM VALUES OF THE COMPRESSOR MODEL'S IDENTIFIED PARAMETERS.

Parameter	Optimum Value
V_s Increment Factor, K	1.0834 [-]
$R_{v,in}$	3.097 [-]
α	0.2532 [-]
ϵ_{su}	0.732 [-]
ϵ_{ex}	0.367 [-]
$\dot{W}_{loss,0}$	262.2 W

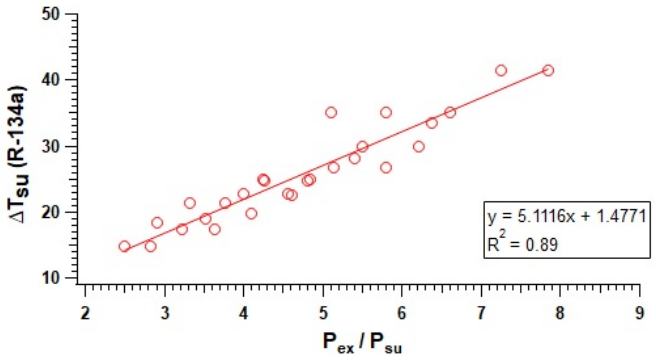

FIGURE 6: PREDICTED VALUES FOR ΔT_{su} FOR INTENDED COPMRESSOR MODEL USING R-134a.

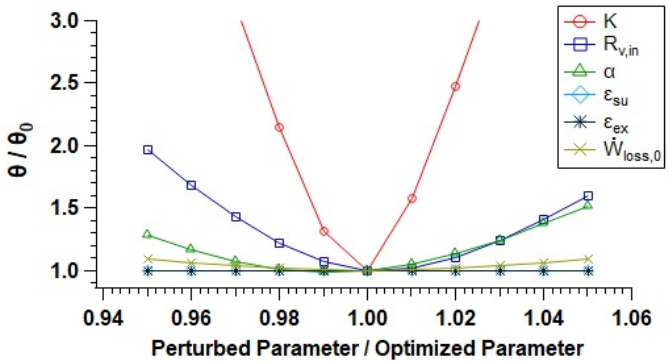

Figure 7: SENSITIVITY ANALYSIS OF COMPRESSOR MODEL PARAMETERS.

5. MODEL VALIDATION

It is intended to use the tuned and tested model to make predictions for choice of working fluids other than those used for generating the data. For this purpose, the tuned model is used to predict the output parameters shown in Figure 2 (except $\dot{Q}_{amb}$). To demonstrate this concept, manufacturer provided data for R-407c is used. These are 62 data points in addition to those for R-134a that are provided by the compressor manufacturer. A strategy for predicting the given compressor performance for working fluids other than the base refrigerant, R-134a, is detailed below.

Note that in the figures that follow, the Root Mean Square Error (RMSE) and the Normalized Root Mean Square Error (NRMSE) are used to gauge the effectiveness of the chosen strategy, which is detailed in three scenarios. The NRMSE is required for a relative comparison of the error between the three parameters, since the RMS error is 'scale-dependent' (as can be seen by the values in the plot legends). The RMS and NRMS errors are computed as shown in Eqs. (39) and (40) below, where the normalization is done based on the minimum and maximum values of the measured variable, Y, where Y could be either one of mass flowrate, compressor shaft power or compressor discharge temperature.

$$\text{RMSE} = \sqrt{\frac{1}{n}\sum_{i=1}^{n}(Y_{pred,i} - Y_{meas,i})^2} \quad (39)$$

$$\text{NRMSE} = \frac{RMSE}{Y_{meas,max} - Y_{meas,min}} \quad (40)$$

Note that the RMS error is the correct metric to use in a prediction/forecasting scenario, where each predicted value is compared against its counterpart measured value. Alternatively, the standard deviation makes more sense when the data has a Gaussian distribution (bell-shaped), while the manufacturer provided data is saw-tooth shaped in nature. This data was used to generate the plots in the current section, but is not cited for the sake of brevity; however, a link to the data is provided in the Acknowledgements.

5.1 Scenario 1: $\Delta T_{su}, \epsilon_{su}, \epsilon_{ex}$ Unchanged

The heat transfer during suction and discharge affect internal and final state of the working fluid flowing through the compressor. These, in turn, are dependent on the two heat exchange effectiveness, ϵ_{su} and ϵ_{ex} and the temperature change during suction. As a first trial, these parameters are not modified for use with R-407c and the base values provided in Table 1 are used. Subsequent results for the compressor mass flow rate, compressor shaft power and refrigerant exhaust temperature are plotted in Figures 8 – 10. Based on the RMSE values reported in the figures, it can be seen that the model predicts the mass flowrate within 3.47 g/s of that reported by the manufacturer. Similarly, the shaft power and exhaust temperature are predicted to within 91.8 W and 24.8°C of the manufacturer values respectively, based on the above strategy.

This result leads to a need to suitably modify one or more of the three parameters being studied (i.e., ΔT_{su}, ϵ_{su} and ϵ_{ex}). However, note that the scale of the parameter under study influences the RMSE value. As such, an RMSE value of 91.8 W is not high, considering that the compressor shaft power is in the kilowatt range. Hence, the normalized root mean square error, or NRMSE, is a better metric to gauge the predictive capabilities of the solution scenario being presented, as described above. Relatively high NRMS errors of 0.025, 0.018 and 0.41 were found for the mass flowrate, shaft power and exhaust temperature, respectively. Thus, further modification of the solution strategy was needed to predict the manufacturer data with greater accuracy as represented by a lower NRMSE.

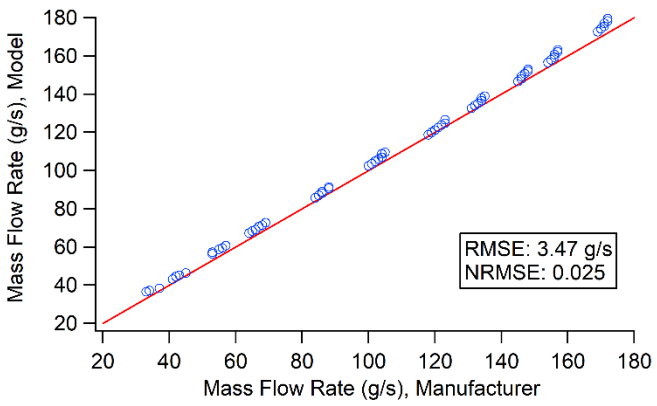

FIGURE 8: EXPERIMENTAL AND PREDICTED MASS FLOW RATE VALUES – SCENARIO 1.

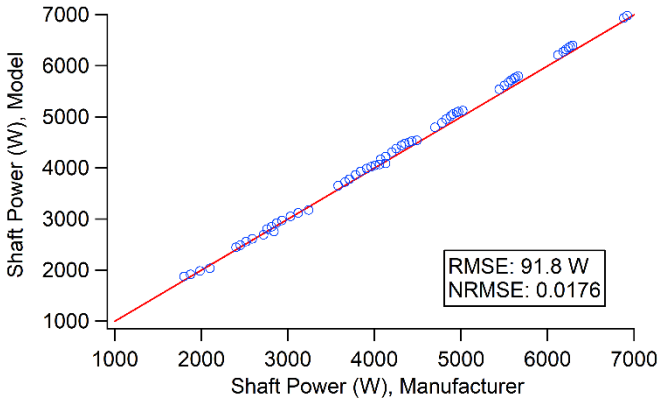

FIGURE 9: EXPERIMENTAL AND PREDICTED SHAFT POWER VALUES – SCENARIO 1.

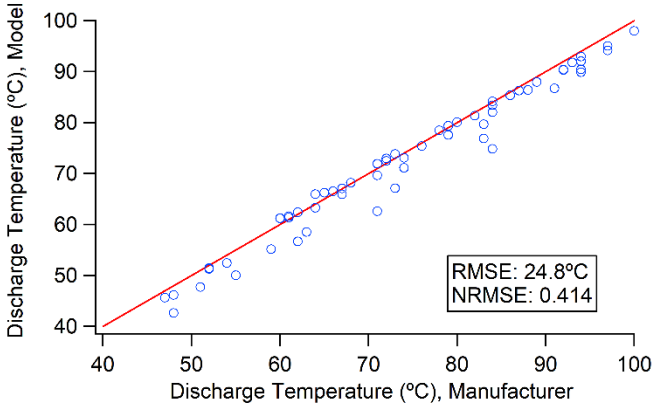

FIGURE 10: EXPERIMENTAL AND PREDICTED DISCHARGE TEMPERATURE VALUES – SCENARIO 1.

5.2 Scenario 2: ΔT_{su} with k ratio, $\epsilon_{su}, \epsilon_{ex}$ Unchanged

This time again, the suction temperature rise alone is modified, but now using a ratio of the ratio of specific heats:

$$\Delta T_{su} = \Delta T_{su,nom} * (k_{R134a}/k_{R407c}) \qquad (41)$$

Results in Figures 11 – 13 show that the RMS and NRMS error for the mass flowrate and compressor exhaust temperature are lower than the previous scenario, but is slightly higher for the compressor shaft power. Hence, the k-ratio multiplier was retained as a modifying factor to ΔT_{su}.

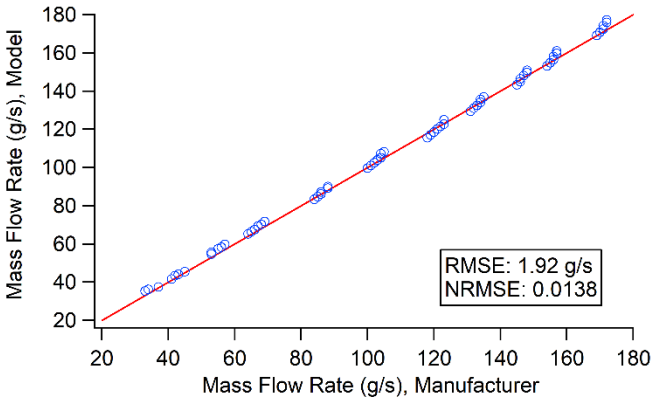

FIGURE 11: EXPERIMENTAL AND PREDICTED MASS FLOW RATE VALUES – SCENARIO 2.

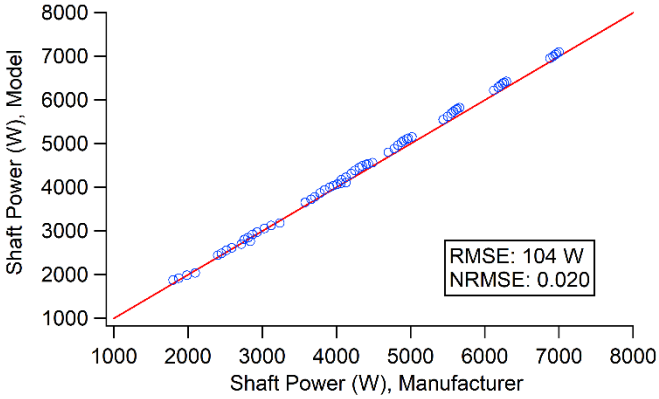

FIGURE 12: EXPERIMENTAL AND PREDICTED SHAFT POWER VALUES – SCENARIO 2.

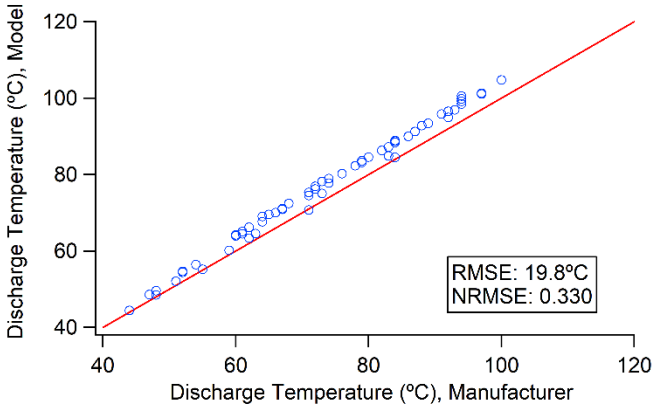

FIGURE 13: EXPERIMENTAL AND PREDICTED DISCHARGE TEMPERATURE VALUES – SCENARIO 2.

5.3 Scenario 3: $\Delta T_{su}, \epsilon_{su}, \epsilon_{ex}$ with k ratio

Lastly, ΔT_{su} is fixed from Scenario 2 while ϵ_{su} and ϵ_{ex} are probed by multiplying them with the ratio of the specific heat ratio of the two fluids similar to Eq. (41). The results of Figures 14 – 16 demonstrate excellent agreement between the predicted and manufacturer specified values for the three output parameters. The RMS error for the compressor exhaust temperature is reduced to 2.1°C, indicating that, on average, the model was able to predict the manufacturer specified exhaust temperature to roughly within 2°C. This yields an NRMSE error of 0.03 for the exhaust temperature. The RMS and NRMS errors for the mass flowrate and compressor shaft power remain the same as in Scenario 2.

In short, using the current technique, the mass flowrate, shaft power and exhaust temperature are predicted to within 1.9 g/s, 103.8 W and 2.1°C, respectively. Accounting for the relative scale of the three parameters, this translates into normalized RMS errors of 0.01, 0.02 and 0.03 respectively.

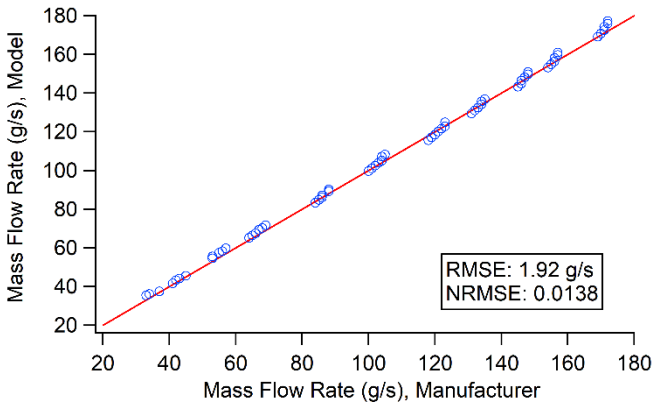

FIGURE 14: EXPERIMENTAL AND PREDICTED MASS FLOW RATE VALUES – SCENARIO 3.

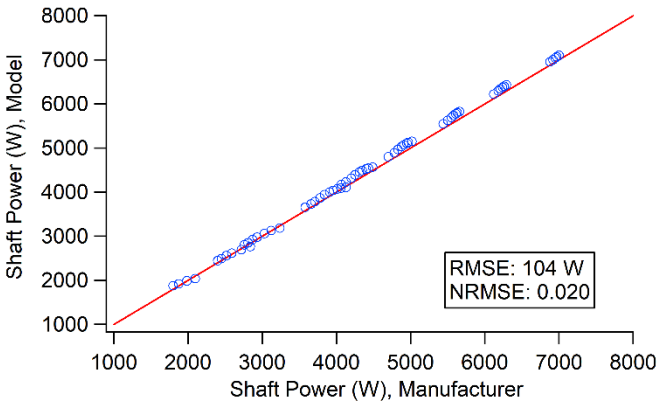

FIGURE 15: EXPERIMENTAL AND PREDICTED SHAFT POWER VALUES – SCENARIO 3.

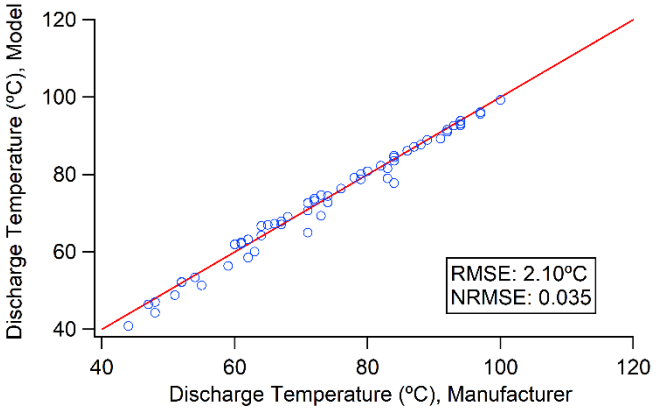

FIGURE 16: EXPERIMENTAL AND PREDICTED DISCHARGE TEMPERATURE VALUES – SCENARIO 3.

Thus, it can be seen from Scenario 3 that the choice of ratios of the specific heat ratio for the base refrigerant, R-134a, to the intended refrigerant, R-407c, predicts the compressor model output variables with the least error. This ratio is applied to modify the suction temperature rise as well as the suction and exhaust heat exchange efficiencies. Transport property values are determined using conditions at suction, point su. In particular, using the NRMS as the error metric, the least error is seen for the mass flow rate, followed by the compressor shaft work and finally the discharge temperature.

6. CONCLUSION

A previously published semi-empirical model of a scroll compressor is modified in this study to predict three primary variables of interest for the scroll compressor and choice of working fluid. The semi-empirical model neglects certain physical aspects such as internal leakage of the refrigerant which occurs between the two scrolls and presence of a discharge valve, typically of the reed type found in scroll compressors. However, since scroll compressors have very high volumetric efficiencies (near 100%), hence leakage can be readily neglected without introducing significant error. Neglecting these two physical aspects keeps the model simple while still maintain a high level of accuracy, as shown by the results of Scenario 3.

ACKNOWLEDGEMENTS

This material is based upon work supported by the NSF IUCRC Award No. IIP-1738782. Any opinions, findings, and conclusions or recommendations expressed in this material are those of the author(s) and do not necessarily reflect the views of the National Science Foundation.

The compressor used for this study is from Emerson Copeland with model # ZR61KCE-TF5-250. The manufacturer performance data for R-134a and R-407c can be found by downloading and installing Emerson's Product Selection software, available at: https://climate.emerson.com/en-us/tools-resources/product-selection-software. Telephone conversations with Emerson Copeland technical support are greatly appreciated in helping to identify the above software and navigating through it to the correct data.

REFERENCES

[1] G. F. Davies, G. G. Maidment, and R. M. Tozer, "Using data centres for combined heating and cooling: An investigation for London," *Appl. Therm. Eng.*, vol. 94, pp. 296–304, Feb. 2016, doi: 10.1016/j.applthermaleng.2015.09.111.

[2] M. Pärssinen, M. Wahlroos, J. Manner, and S. Syri, "Waste heat from data centers: An investment analysis," *Sustain. Cities Soc.*, vol. 44, pp. 428–444, Jan. 2019, doi: 10.1016/j.scs.2018.10.023.

[3] R. Miller, "Using Servers to Heat Homes: Facebook Embraces Heat Recycling," *Data Center Frontier*, Sep. 05, 2017. https://datacenterfrontier.com/using-servers-to-heat-homes-facebook-embraces-heat-recycling/ (accessed Jun. 04, 2020).

[4] P. Zhang, B. Wang, W. Wu, W. Shi, and X. Li, "Heat recovery from Internet data centers for space heating based on an integrated air conditioner with thermosyphon," *Renew. Energy*, vol. 80, pp. 396–406, Aug. 2015, doi: 10.1016/j.renene.2015.02.032.

[5] M. Deymi-Dashtebayaz and S. V. Namanlo, "Potentiometric and economic analysis of using air and water-side economizers for data center cooling based on various weather conditions," *Int. J. Refrig.*, vol. 99, pp. 213–225, Mar. 2019, doi: 10.1016/j.ijrefrig.2019.01.011.

[6] M. Deymi-Dashtebayaz and S. Valipour-Namanlo, "Thermoeconomic and environmental feasibility of waste heat recovery of a data center using air source heat pump," *J. Clean. Prod.*, vol. 219, pp. 117–126, May 2019, doi: 10.1016/j.jclepro.2019.02.061.

[7] E. Oró, R. Allepuz, I. Martorell, and J. Salom, "Design and economic analysis of liquid cooled data centres for waste heat recovery: A case study for an indoor swimming pool," *Sustain. Cities Soc.*, vol. 36, pp. 185–203, Jan. 2018, doi: 10.1016/j.scs.2017.10.012.

[8] K. Ebrahimi, G. F. Jones, and A. S. Fleischer, “A review of data center cooling technology, operating conditions and the corresponding low-grade waste heat recovery opportunities,” *Renew. Sustain. Energy Rev.*, vol. 31, pp. 622–638, Mar. 2014, doi: 10.1016/j.rser.2013.12.007.

[9] Y. Wang and N. Lior, “Thermoeconomic analysis of a low-temperature multi-effect thermal desalination system coupled with an absorption heat pump,” *Energy*, vol. 36, no. 6, pp. 3878–3887, Jun. 2011, doi: 10.1016/j.energy.2010.09.028.

[10] H. R. Datsgerdi and H. T. Chua, “Thermo-economic analysis of low-grade heat driven multi-effect distillation based desalination processes,” *Desalination*, vol. 448, pp. 36–48, Dec. 2018, doi: 10.1016/j.desal.2018.09.018.

[11] R. Miller, “Rack Density Keeps Rising at Enterprise Data Centers,” *Data Center Frontier*, Apr. 27, 2020. https://datacenterfrontier.com/rack-density-keeps-rising-at-enterprise-data-centers/ (accessed Jun. 04, 2020).

[12] R. Khalid, S. G. Schon, A. Ortega, and A. P. Wemhoff, “Waste Heat Recovery Using Coupled 2-Phase Cooling Heat-Pump Driven Absorption Refrigeration,” in *2019 18th IEEE Intersociety Conference on Thermal and Thermomechanical Phenomena in Electronic Systems (ITherm)*, May 2019, pp. 684–692. doi: 10.1109/ITHERM.2019.8757465.

[13] E. Winandy, C. S. Saavedra O, and J. Lebrun, “Experimental analysis and simplified modelling of a hermetic scroll refrigeration compressor,” *Appl. Therm. Eng.*, vol. 22, no. 2, pp. 107–120, 2002, doi: 10.1016/S1359-4311(01)00083-7.

[14] P. Byrne, J. Miriel, and Y. Lenat, “Design and simulation of a heat pump for simultaneous heating and cooling using HFC or CO2 as a working fluid,” *Int. J. Refrig.*, vol. 32, no. 7, pp. 1711–1723, Nov. 2009, doi: 10.1016/j.ijrefrig.2009.05.008.

[15] N. Halm, “Mathematical Modeling of Scroll Compressors,” MS, Purdue University, 1997.

[16] Y. Chen, “Mathematical Modeling of Scroll Compressors,” Doctoral, Purdue University, 2000.

[17] B. Wang, X. Li, and W. Shi, “A general geometrical model of scroll compressors based on discretional initial angles of involute,” *Int. J. Refrig.*, vol. 28, no. 6, pp. 958–966, 2005, doi: 10.1016/j.ijrefrig.2005.01.015.

[18] E. Oralli, M. A. Tarique, C. Zamfirescu, and I. Dincer, “A study on scroll compressor conversion into expander for Rankine cycles,” *Int. J. Low-Carbon Technol.*, vol. 6, no. 3, pp. 200–206, Sep. 2011, doi: 10.1093/ijlct/ctr008.

[19] C. Cuevas, J. Lebrun, V. Lemort, and E. Winandy, “Characterization of a scroll compressor under extended operating conditions,” *Appl. Therm. Eng.*, vol. 30, no. 6–7, pp. 605–615, 2010, doi: 10.1016/j.applthermaleng.2009.11.005.

[20] V. Lemort, “Contribution to the Characterization of Scroll Machines in Compressor and Expander Modes,” Ph.D. Dissertation, University of Liege, Liege, Belgium, 2008.

[21] P. Techarungpaisan, S. Theerakulpisut, and S. Priprem, “Modeling of a split type air conditioner with integrated water heater,” *Energy Convers. Manag.*, vol. 48, no. 4, pp. 1222–1237, Apr. 2007, doi: 10.1016/j.enconman.2006.10.012.

[22] E. Kinab, D. Marchio, P. Rivière, and A. Zoughaib, “Reversible heat pump model for seasonal performance optimization,” *Energy Build.*, vol. 42, no. 12, pp. 2269–2280, Dec. 2010, doi: 10.1016/j.enbuild.2010.07.007.

[23] P. Byrne, J. Miriel, and Y. Lénat, “Modelling and simulation of a heat pump for simultaneous heating and cooling,” *Build. Simul.*, vol. 5, no. 3, pp. 219–232, Sep. 2012, doi: 10.1007/s12273-012-0089-0.

[24] J. P. Bourdouxhe, M. Grodent, and J. J. Lebrun, “A Toolkit for Primary HVAC System Energy Calculation – Part 2: Reciprocating Chiller Models,” *ASHRAE Trans.*, vol. 100, no. 2, pp. 774–786, 1994.

[25] F. P. Incropera and F. P. Incropera, Eds., *Fundamentals of heat and mass transfer*, 6th ed. Hoboken, NJ: John Wiley, 2007.